Progress in Organic Coatings 189 (2024) 108357

Contents lists available at ScienceDirect

Progress in Organic Coatings

journal homepage: www.elsevier.com/locate/porgcoat

Exploring the role of passivating conversion coatings in enhancing the durability of organic-coated steel against filiform corrosion using an electrochemical simulated approach

Andrea Cristoforetti *, Stefano Rossi, Flavio Deflorian, Michele Fedel

Department of Industrial Engineering, University of Trento, via Sommarive n. 9, 38123 Trento, Italy

ARTICLE INFO

Keywords:
Steel
Conversion coatings
Filiform corrosion
Electrochemical characterization
Corrosion resistance
Organic coatings

ABSTRACT

This study investigates the effectiveness of conversion coatings (CCs) in mitigating filiform corrosion (FFC) on acrylic-coated steel substrates, with a specific focus on iron phosphatizing and trivalent chromium conversion coatings. Aiming to evaluate the effectiveness of a simulated electrochemical approach introduced in a previous publication, several parameters are determined through an approach involving potentiodynamic polarization curves and zero resistance ammeter on bare CCs. These experiments are conducted in test solutions designed to replicate the electrolytic conditions the substrate encounters undergoing FFC. Similar measurements are collected in neutral testing solutions and the outcomes of the two approaches are discussed regarding the performances of the organic coated sample. The electrochemical evaluation of CCs highlights their potential to reduce the driving forces and nucleation tendency. However, for the steel coated with acrylic paint, while CCs reduce the initiation sites for delamination, they have limited impact on filament propagation.

1. Introduction

Filiform corrosion (FFC) represents a superficial, filament-like corrosion phenomenon that occurs beneath coatings, predominantly on metal surfaces, including steel [1,2]. In this latter case, FFC filament comprises two distinct components: (i) a head region containing a blend of intermediate corrosion products known as green rust [3,4], and (ii) an extending tail primarily composed of hydroxides. FFC advances through an anodic undermining process at the metal-paint interface, driven by a differential aeration cell along the filament's length [5,6].

The appearance of FFC is a result of a multifaceted interplay of factors, including the moisture level within a specific range of 65–93 % relative humidity [7,8], the existence of coating defects that expose the underlying metal to salts, the presence of intermetallic particles, and the availability of oxygen [6,9].

As detailed in a previous publication [9], FFC can be conceptualized as an electrochemical process, wherein the anodic and cathodic regions are distinctly separated. The exchange of charge between these regions can be regarded as the corrosion current. The two active sites were demonstrated to be spatially defined and well-distinct along the threads [10]. Anode and cathode are separated by a poorly defined membrane [11] similar to the one described by Van der Weijde et al. [12] in the case of cathodic delamination on coated iron. Moreover, adherence to the principle of charge conservation necessitates that the cumulative reduction currents must equate to the sum of all oxidation currents, thus preventing the accumulation of charge. Consistent with this theoretical framework, the potential difference resulting from varying aeration conditions can be regarded as the driving force behind the progression of FFC, denoted as ΔE_{FFC}. Meanwhile, the current density ($i_{CORR\ FFC}$) can be considered a parameter associated with the propagation of this corrosion phenomenon.

The impact of filiform corrosion on the structural integrity of metallic products is generally not considered detrimental. However, it triggers paint detachment, thus making the protective coating much less effective, and potentially facilitating a more extensive corrosive process. Therefore, the significance of preventing and mitigating this failure to improve the coated system's durability is evident. Furthermore, the gradual alteration of the appearance of painted items over time is no longer deemed acceptable. Any deviation from the desired appearance directly influences maintenance expenses and the frequency of scheduled servicing events. However, it is noteworthy that there is a paucity of clear, universally accepted guidelines for effectively preventing this

* Corresponding author.
E-mail addresses: andrea.cristoforetti@unitn.it (A. Cristoforetti), stefano.rossi@unitn.it (S. Rossi), flavio.deflorian@unitn.it (F. Deflorian), michele.fedel@unitn.it (M. Fedel).

https://doi.org/10.1016/j.porgcoat.2024.108357
Received 28 December 2023; Received in revised form 6 February 2024; Accepted 22 February 2024

phenomenon on coated steel surfaces, and it is seldom given due consideration.

In this work, a common corrosion mitigation technique, known as surface conversion, was examined against FFC. Surface conversion is a frequently employed method within the domain of protective coatings, predominantly utilized to augment substrate compatibility prior to coating application [13–24]. Once the metal is properly cleaned, an application of a thin, insoluble, and well-adherent layer can beneficially modify the surface characteristic. Higher roughness, improved chemical stability, and easier bonding formation with the organic layer are the main features on which the conversion coatings (CCs) rely. In light of the inescapable water and ions permeability exhibited by organic coatings [25,26], CCs efficiently mitigate electrochemical processes occurring at the interface, particularly those linked to paint delamination and underpaint corrosion. The properties of general CCs are able to provide a certain restriction upon electron transfer between anodic and cathodic sites [14,27,28]. By harnessing the potential of CCs and considering their strategic placement within a coating system, their aptitude for mitigating FFC becomes a salient feature. Extensive research has been conducted to examine the influence of multiple conversion coatings on the manifestation of FFC, specifically on aluminum substrates coated with organic coatings, yielding encouraging findings [22,29–36,65]. However, to the best of current knowledge, there is no available reference concerning the utilization of CCs in painted steel protection with a specific focus on FFC. Hence, in the context of this investigation, two commercially employed corrosion inhibitors, widely embraced within the industrial sector for the pretreatment of steel surfaces, have been examined as potential strategies for mitigating FFC on acrylic-coated steel. This research aimed to fill this gap in painted goods failure knowledge.

Iron phosphatizing has been widely used for decades as an alternative to chromium-based baths. This technology relies on the deposition of insoluble heavy metal ternary phosphate [37,38]. The non-conductive nature of the deposited layer limits and postpones the occurrence of corrosion. Another technology commercially available since 2000 is the trivalent chromium CC (Cr(III)). This thin film can impede oxygen transport to the surface, but unlike the precursor hexavalent one (Cr(VI)), no healing properties are provided. Both the aforementioned conversion coatings (CCs), their formation mechanisms, and overall corrosion resistance have been subject to extensive research over the years. This study did not seek to contribute additional insights into the pretreatment technologies themselves. In fact, the primary emphasis was on exploring their suitability for a new application: addressing FFC on surfaces coated with organic layers. In addition, this study employed the electrochemical characterization technique introduced in a recent publication [9] to assess the FFC resistance of the previously described CCs.

With this focus, after a complete general electrochemical characterization in a neutral environment based on potentiodynamic polarization (PDP) and electrochemical impedance spectroscopy (EIS), a specific experimental campaign was dedicated to the FFC resistance. An electrolyte-simulated approach (described in [9]) was adopted to assess the treated metallic surface's durability performances in the anodic and cathodic FFC environment. Coupling PDP and zero resistance ammeter (ZRA) results, collected in the so-called anolyte and catholyte testing solutions, an estimation of the improvements given by iron phosphatizing and Cr(III) thin coatings with respect to the untreated bare steel was achieved. Finally, acrylic-coated pretreated steel panels were produced and aged following the FFC test (80 % r.h. at 40 °C after NaCl contamination) [39]. Their degradation extent was discussed in comparison with the untread reference in terms of filament nucleation susceptibility and propagation rate. Furthermore, some morphological modifications of the FFC and mechanism alteration were detected by optical imaging monitoring.

2. Materials and methods

2.1. Experimental

2.1.1. Conversion treatments

The CCs were applied on steel samples made of R36 Q-Panels Steel A1008 (C max. 0.15 wt%; Mn max. 0.6 wt%; P max. 0.03 wt%; S max 0.035 wt%, and Fe. bal.). The cold rolled low carbon steel panels are characterized by a surface roughness comprised in the 0.63–1.65 μm range. In the prior pretreatment stage, each steel substrate underwent degreasing with sonicated acetone, followed by immersion in an acid solution containing 80 g/L of HCl for a duration of 15 min. The pretreatments used in the process include commercially available BONDERITE M-FE 1070 iron phosphate (referred to as "Phosphate") and BONDERITE M-NT 5992 (referred to as "Cr(III)") supplied by Henkel (Düsseldorf, Germany). The choice of the CC technologies was made along the commonly utilized baths in the industrial field for steel structures [14,37,40]. The CCs were applied following the instructions provided by the supplier. The Cr(III) bath was prepared according to the manufacturer's specifications, achieving a pH of 3.5. The pretreatment solution was applied by spray at room temperature, followed by a drying stage in the oven at 100 °C for 1 h (no rinse treatment). The Phosphate bath was adjusted at pH 5 by NaOH solution and applied by immersion for 5 min at 45 °C. Subsequently, a thorough rinse with demineralized water was performed, followed by air-drying at room temperature for a duration of one hour. SEM JEOL IT 300 instrument was employed to investigate the modified surface morphology and chemical composition.

2.1.2. Conversion coatings characterization

Electrochemical tests such as EIS and potentiodynamic analysis were performed both on the untreated and converted surfaces using an Autolab PGSTAT302N potentiostat. EIS measurements were carried out at room temperature in a NaCl 0.5 M aqueous solution with a neutral pH (6.2), applying a signal amplitude of 10 mV in a frequency range from 100 kHz to 10 MHz after 2 h of immersion (aerated condition). An Avesta-type cell with a platinum counter electrode and an Ag/AgCl/3.5 M KCl reference electrode was used. A circular testing area of 1 cm^2 was exposed to the electrolyte. Zsimpwin® software was employed to analyze the EIS raw data set with the equivalent electric circuits (EEC). In the case of potentiodynamic analysis, the samples were tested at a scan rate of 0.2 mV/s, over the range − 300 + 900 mV vs. open-circuit potential (OCP). The same testing geometry described for the EIS test was adopted, with the same area and electrolytic solution. The analysis was performed at room temperature after waiting 2 h. This delay period was chosen after the OCP monitoring upon stabilization.

Following the experimental approach proposed in the previous publication [9], the pretreated steel surfaces were characterized for their susceptibility to FFC. Given that the FFC's active head consists of two distinct environments characterized by the presence of ions, oxygen availability, and pH levels, the potentiodynamic curves' anodic and cathodic branches were collected separately in two unique electrolytes, referred to as anolyte and catholyte. The composition of these simulated electrolytes is reported in Table 1. The anolyte comprises 0.1 M $FeCl_3$, as it is anticipated that some iron dissolution will occur at the anodic site [10]. This concentration of iron salt aligns with previously reported studies on aluminum in the literature [11,41]. The pH was adjusted to 1.5 by gradually adding 33 % HCl, in accordance with previous

Table 1
Anolyte and catholyte compositions and features.

Testing solutions	Anolyte	Catholyte
pH	1.5	12
Ions	Fe^{3+}, Cl^-, H^+	Na^+, OH^-
Oxygen (ppm)	1.4	7.5
T (°C)	40	40

literature reports [42,43]. Recognizing that the cathodic site likely experiences reduced oxygen concentration due to limited availability, high ionic strength, and a lower pH, the anolyte was continuously purged with nitrogen to reduce the dissolved oxygen (DO) to approximately 1.4 ppm, as described in prior studies [41,44]. Since the cathodic reaction leads to localized alkalinization resulting from the oxygen reduction reaction on the steel substrate ($4Fe^{2+} + O_2 + 2H_2O \rightarrow 4Fe^{3+} + 4OH^-$) [9,10], the catholyte was replicated using a NaOH aqueous solution with a pH of 12 [5,45]. This setup was expected to induce passivation of the steel surface [46]. Continuous air bubbling was applied to stabilize the DO levels in the electrolyte.

The open circuit potential of the treated surfaces was monitored for 160 min for surface stabilization in the two simulating environments. The following polarization curves were collected after a wait time of 2 h. The anodic and cathodic branches were obtained by polarizing from −50 mV to +300 mV under nitrogen bubbling and from +50 mV to −300 mV (with air insufflation) with respect to the OCP. All electrochemical measurements were conducted under a consistently maintained temperature of 40 °C, ensuring a standardized environment in accordance with the established conditions of the FFC standard testing.

Moreover, the anode and cathode sites of the filament were simulated in two different cells connected with a jelly agar-saturated KCl salt bridge to perform ZRA measurements. The current flow between the two treated steel samples placed in the N_2 bubbled anolyte, and synthetic air fluxed catholyte was measured. The samples were simply immersed in the respective solution. ZRA's setup details were introduced elsewhere [9]. The ZRA measurement was configured to run for a period of 2 h, and after an initial few minutes during which the current stabilizes, the average value of the last hour was recorded.

2.1.3. Coated sample production and characterization

The steel substrates underwent a coating process using an acrylic-based clearcoat supplied by Palini Vernici (Pisogne BS, Italy). The selection of the clear coat was made with the intent of enabling a visual examination of the corroding interface between the metal substrate and the paint layer. The coating application was conducted using a blade apparatus known as the Elcometer 4340 Automatic Film Applicator. A dry film thickness of 75 μm was obtained by curing at 60 °C in an oven for 1 h, achieving a glass transition temperature of 46 °C [47]. The coated specimens were prepared in accordance with the ASTM 2803 standard [39]. Prior to exposure within the neutral salt spray chamber, in compliance with ASTM B117 standard [48] for 5 h, a scribe measuring 1 mm in width and 60 mm in length was made in the coating. The introduction of chloride ions into the scratch is essential for initiating FFC [39]. Filament propagation was promoted by placing the specimens in a controlled environment at 40 °C with a relative humidity of 80 % [39]. These carefully controlled humidity conditions encourage filament development, which was periodically observed using optical imaging techniques. The software ImageJ was used for the determination of the corroded area and to monitor the corrosion rate.

3. Results and discussion

When subjected to phosphatizing (Fig. 1b), the steel surface displays a macroscopically uniform appearance. In contrast, the Cr(III) conversion treatment does not exhibit homogeneous treatment. The observed irregularities are attributed to the no-rinse technology, in which the drying of the liquid chemicals left on the steel surface results in a non-uniform degree of deposition.

In both instances, the deposited morphology exhibited a texture of shapes with dimensions on the order of 100 nm as shown in Fig. 2. The phosphate-based chemical conversion developed on the etched steel surface due to the acidic nature of the conversion bath. The resultant structure exhibits uniform growth in size and spatial distribution (Fig. 2b), highlighting distinctive features characteristic of such treatment [49–51]. In the case of Cr(III), a micro-rougher surface is achieved, and the deposits seem unevenly distributed, resulting in smoother pristine regions and textured converted areas, as supported by macroscopic observations (Fig. 2a). Notably, some cracks are discernible in the outer layer [40].

In this study, electrochemical tests are carried out at two distinct investigative levels. Initially, EIS is utilized to comprehensively evaluate the barrier properties of the conversion layer and assess its enhancement compared to bare metal. Following this, PDP and ZRA are integrated to simulate the specific conditions arising from an anodic undermining process. The electrochemical assessment of treated surfaces in a neutral saline environment reveals that both conversion coatings (CCs) exhibit enhanced durability compared to untreated bare steel. Concerning the EIS outcomes provided in Fig. 3, the two pretreatments markedly increase the impedance modulus in the low-frequency range. When examining the data collected at 0.01 Hz, it appears that the Phosphate coating exhibits a slightly superior performance. This observation is further supported by the charge transfer resistance (R_{ct}) obtained from the EIS raw data sets, which have been fitted using a basic R(QR) Randles circuit (as shown in Fig. 3b insert), indicating the presence of a single-time constant [52,53]. The term Q or constant phase element (CPE) takes into account the deviation from a pure capacity behavior of the electrical double layer at the metal-electrolyte interface [52,54].

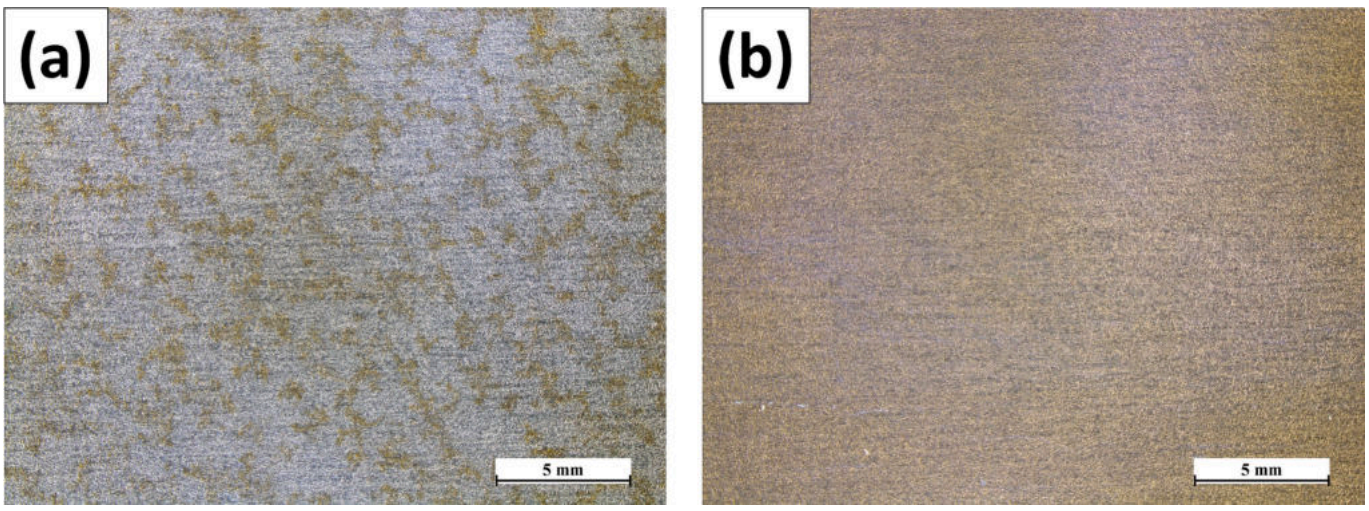

Fig. 1. Optical image of the steel surface after the conversion stage. (a) Details the Cr(III) no-rinse treatment deposits, while (b) shows the surface after phosphatizing.

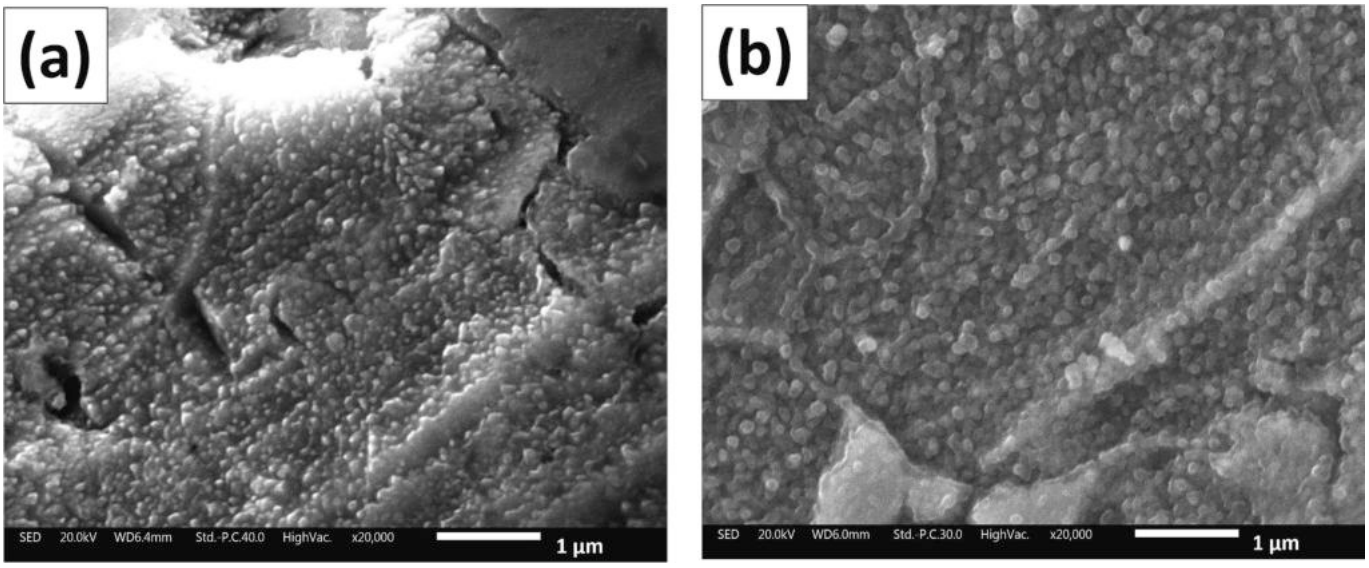

Fig. 2. SEM-SED images of Cr(III)-treated (a) phosphate-treated (b).

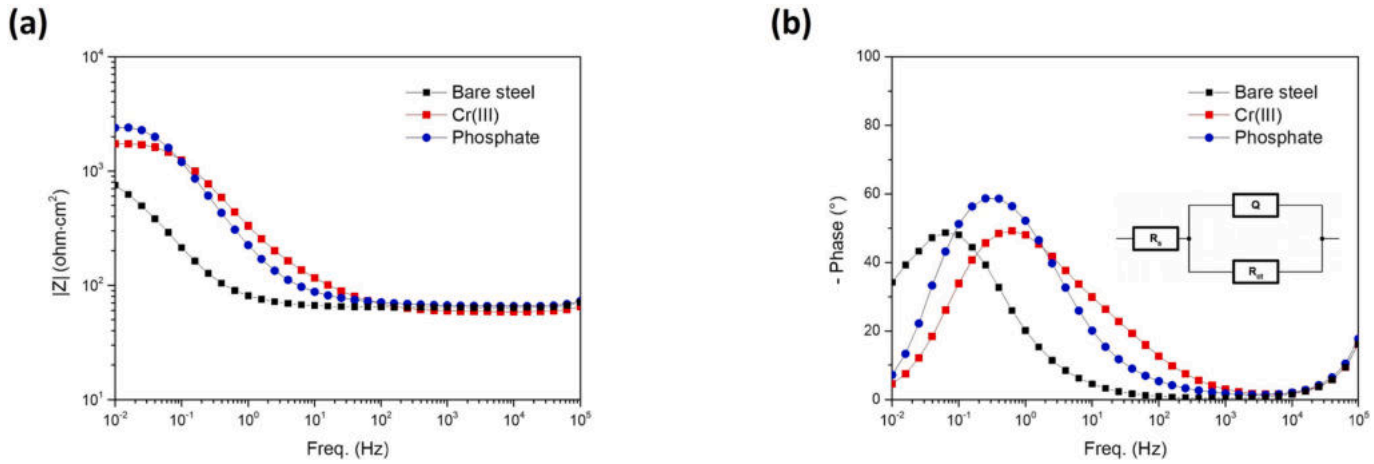

Fig. 3. EIS diagrams of impedance modulus (a) and phase angle (b) collected on bare steel and treated steel with Cr(III) and Phosphate conversion coatings.

This method has been employed to simulate the behavior of heterogeneous surfaces, in contrast to the conventional use of double-layer capacitance C_{dl}, which is typically suited for electrodes with homogeneous surfaces. The fitting outcomes are reported in Table 2. Y_0 and n are the admittance and exponent parameters, respectively, constituting the Q according to Eq. (1), where ω is the angular frequency (rad s^{-1}).

$$Q(\omega) = [Y_0(j\omega)^n]^{-1} \quad (1)$$

The effective capacitance of the double layer can be derived from CPE parameters and charge transfer resistance by Eq. (2) [55]:

$$C_{dl} = \frac{(R_{ct}Y_0)^{1/n}}{R_{ct}} \quad (2)$$

Nevertheless, it is crucial to note that when the exponential term "n" significantly deviates from the condition of pure capacitance ($n = 1$), the interpretation of the data becomes unreliable, and it is not possible to attribute a clear physical meaning to the Y_0 parameter. The Phosphate coating seems able to provide a higher charge transfer resistance (R_{ct}), thus significantly improving the corrosion resistance by means of a redox reaction slowdown.

Table 2
Equivalent electrical parameters obtained from the fitting of EIS raw data sets.

Sample	R_{ct} (kΩ·cm²)	Y_0 (μS^n Ω^{-1} cm^{-2})	n
Bare steel	1.25	8450	0.72
Cr(III)	1.98	769	0.74
Phosphate	2.78	1060	0.84

Analyzing the PDP curves (Fig. 4) collected in the same environment after a similar immersion time (2 h), both the CCs induce an increase in the corrosion potential of about +100 mV for Cr(III) and + 70 mV for Phosphate. Moreover, after conversion treatments, the anodic current decreases by about one order of magnitude with respect to the bare steel, implying an enhanced corrosion resistance. These outcomes are in line with the EIS results and confirm the effectiveness of the corrosion protection provided by CCs in near-neutral conditions.

After assessing the actual performance in a neutral environment, the electrochemical analysis is extended to encompass two electrolytes that replicate the anolyte and catholyte environments, and the correspondence with the actual FFC susceptibility is discussed.

Open circuit potential vs time curves are collected over the pretreated steel samples in different testing solutions. The measurements suggest that the stabilization time for the investigated samples is about 2 h.

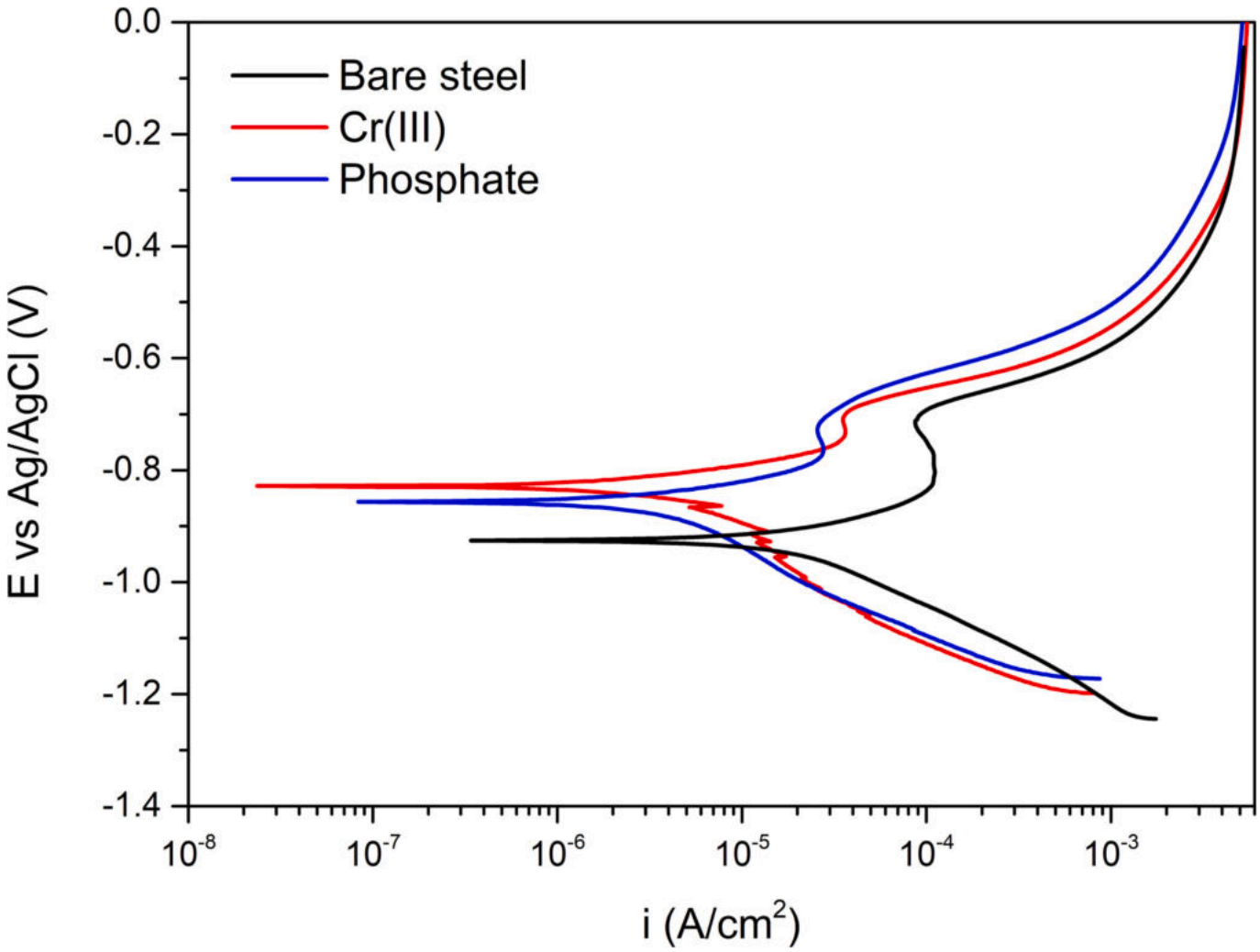

Fig. 4. Potentiodynamic polarization curves collected on bare steel and treated steel with Cr(III) and Phosphate conversion coatings.

It is worth noting that both samples in the anolyte exhibit a more noisy behavior, suggesting heightened reactivity within this acidic environment compared to the passivating conditions in the catholyte. Furthermore, Fig. 5 provides a first estimation of the decrease in the difference of potential established between the anode and the cathode during FFC, which has been previously measured to be 0.230 V on bare steel [9]. The Cr(III) accounts for a reduction of 87 %, while Phosphate for 65 % of that electrochemical driving force.

The same discussion can be made on the PDP curves in Fig. 6, dealing with the difference in the corrosion potential between the anodic and cathodic branches. The values of the parameters representing the FFC driving force are provided in Table 3. CCs act mainly on the activity in

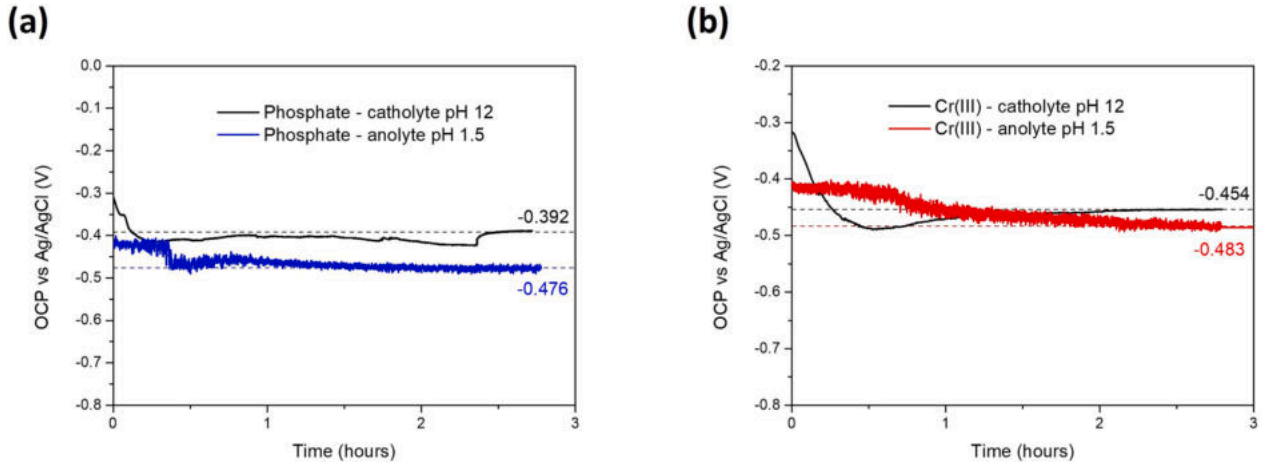

Fig. 5. Open circuit potential monitoring of phosphate coating and Cr(III) coatings in anolyte/catholyte simulated electrolytes.

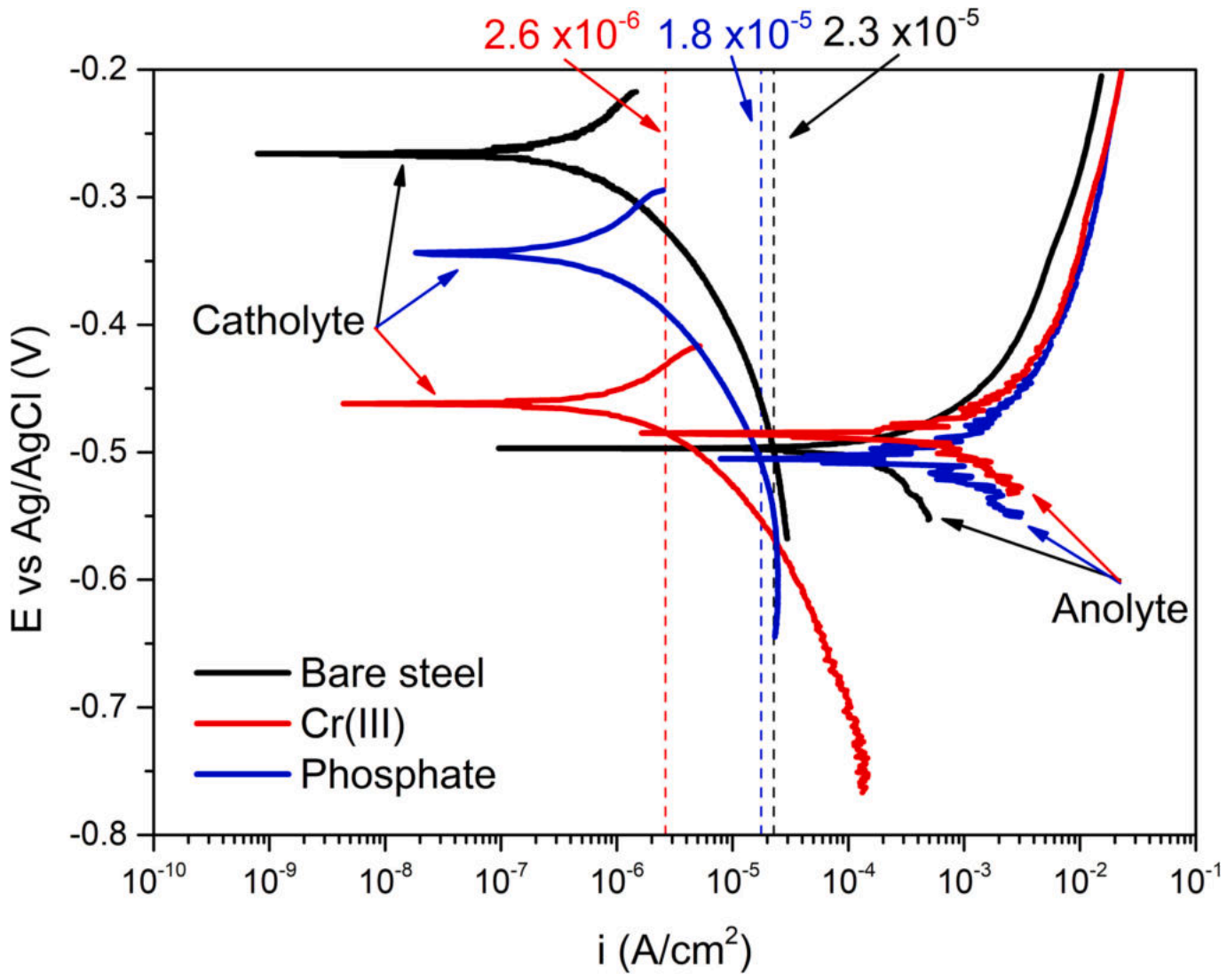

Fig. 6. Potentiodynamic polarization curves on bare steel, phosphate coating, and Cr(III) coatings collected in anolyte/catholyte simulated electrolytes.

Table 3
Electrochemical parameters derived from the potentiodynamic polarization curves collected in anolyte/catholyte simulated electrolytes. Mean values obtained from replicate measurements are reported.

PDP	$i_{CORR\ FFC}$ (μA/cm^2)	ΔE_{CORR} (V)
Bare steel	19 ± 3	0.23 ± 0.01
Cr(III)	6.7 ± 2.0	0.027 ± 0.009
Phosphate	18.7 ± 3.6	0.142 ± 0.010

catholyte, and the shift of these branches leads to a drop in filiform corrosion current of 65 % for Cr(III), while for Phosphate this parameter results comparable to the untreated sample. Due to the presence of nanoscale defects in thin conversion films, oxygen reduction occurs at the metal/electrolyte interface, resembling a scenario observed with microelectrode arrays. Consequently, such measurements are limited to offering only a qualitative assessment of the hindrance effect on oxygen reduction [56,57].

Concerning the behavior in the anolyte (acidic environment), no significant differences for the CCs with respect to the bare steel can be observed. This finding suggests poor stability of the CCs at low pH it suggests the damaging effect that the considered environment causes on the converted surfaces. Replicates of the PDP curves presented are provided in Appendix A1 and A2. Thin film performances seem better in the alkaline conditions typical of the catholyte. However, the primary concern regarding the suitability of these CCs against FFC centers around the observation that the foremost event during coating delamination is of an anodic nature. Given the acknowledged instability of the deposited thin films in such conditions, it becomes challenging for the CCs to effectively mitigate cathodic events, particularly if they manifest in the filament tail following the initial anodic head. In this scenario, the cathodic sites are situated within an already compromised portion of the treated surface, owing to the prior exposure to the corrosive acidic liquid environment at the advancing head of the corrosion. However, considering that FFC involves an initial nucleation stage driven by cathodic activity in the defective coating, the behavior exhibited by the CCs in Fig. 6 could prove effective during this early phase of the corrosion mechanism.

In this sense, also the reliability of the electrochemical simulated data could likely be less significant since the kinetic ($i_{corr\ FFC}$) and thermodynamic (ΔE_{CORR}) parameters are mainly determined by the effect experienced by the integer CCs in contact with the catholyte environment, a scenario not possible to be found in the real FFC propagation.

The second approach exploited to simulate the FFC mechanism from an electrochemical point of view is the ZRA. To validate the findings from the previous tests, the corrosion current between the two cells

emulating the anode and cathode is quantified. The values derived from Fig. 7 upon current stabilization are shown in the inset. The substrate ranking of the electrochemical activity is in agreement with the PDPs outcomes. Both the CCs effectively shelter the substrate, decreasing $i_{ZRA\ FFC}$ by 94 % and 68 % concerning Cr(III) and Phosphate, respectively. According to the findings, both the CCs enhance the corrosion resistance, and Cr(III) seems to better mitigate FFC. However, also in this case the simulated configuration could differ from the real FFC model in the integrity of the deposited films when acting as a cathode in the filament tail [10]. Comparable remarks regarding the representativeness of simulated electrochemical outcomes arise when addressing the stability issues of the CCs verified to be unstable in an anodic environment. These observations parallel the considerations made earlier concerning potentiodynamic curves. Replicas of the ZRA measurements are provided in Appendix A3.

Summarizing the electrochemical outcomes, neither experiments in a neutral testing solution nor those reproducing the electrolyte developing during FFC are expected to faithfully simulate the actual scenario during filament growth. Nonetheless, the beneficial effect of the treatments is suggested from various points of view, but it could be supposed to be related more to the cathodic activity and thus act more on the FFC initiation stage [8].

The converted surfaces are subjected to corrosion protection testing in combination with an acrylic-based clearcoat. The dry adhesion of the coating is evaluated. An image of the adhesive failures that occurred on all the tested samples is shown in Fig. 8. The conversion coatings do not increase the bonding between the steel and the paint as expected: 3.4 MPa is measured for the untreated sample. Cr(III) coated samples fail at a mean load of 2.5 MPa, while Phosphate withstands up to 3.4 MPa. It is essential to note that wet adhesion (or resistance to delamination) may not be directly synonymous with the bonding strength determined in the Pull-off test. This distinction is due to water uptake and the following electrochemical reactions beneath the paint surface [58,59].

Three sets of scratched-coated samples are aged for each substrate as part of the filiform corrosion test [39]. The transparency of the coating allows for the continuous monitoring of under-paint corrosion over time, enabling the observation of susceptibility at the initiation of FFC and the subsequent propagation of filaments. Fig. 9 displays the average number of filaments per unit length that developed from the longitudinal scribe after being exposed for 100 h under constant conditions of 80 % relative humidity at 40 °C. Both CCs exhibit a noticeable reduction in their propensity for nucleation of filaments when compared to the unconverted coated substrate, denoted as “Bare steel”. A comparison

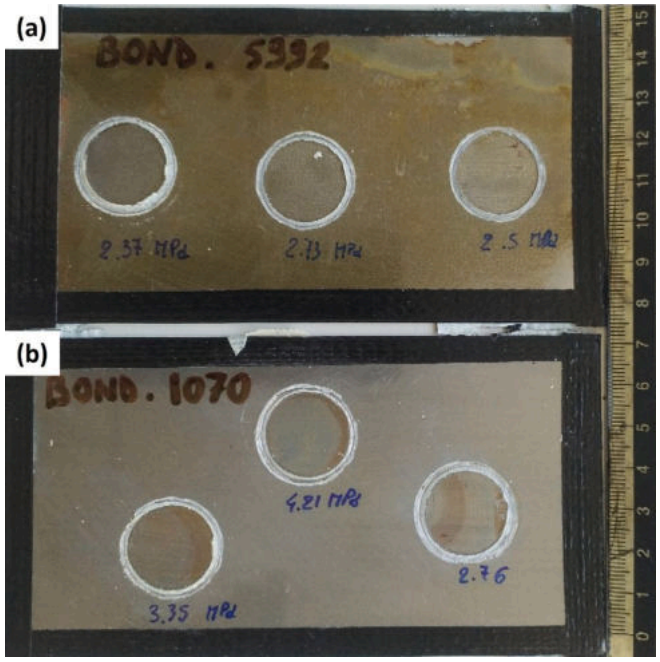

Fig. 8. Tested samples after pull-off dry adhesion test. (a) refers to Cr(III) and (b) to phosphate coating.

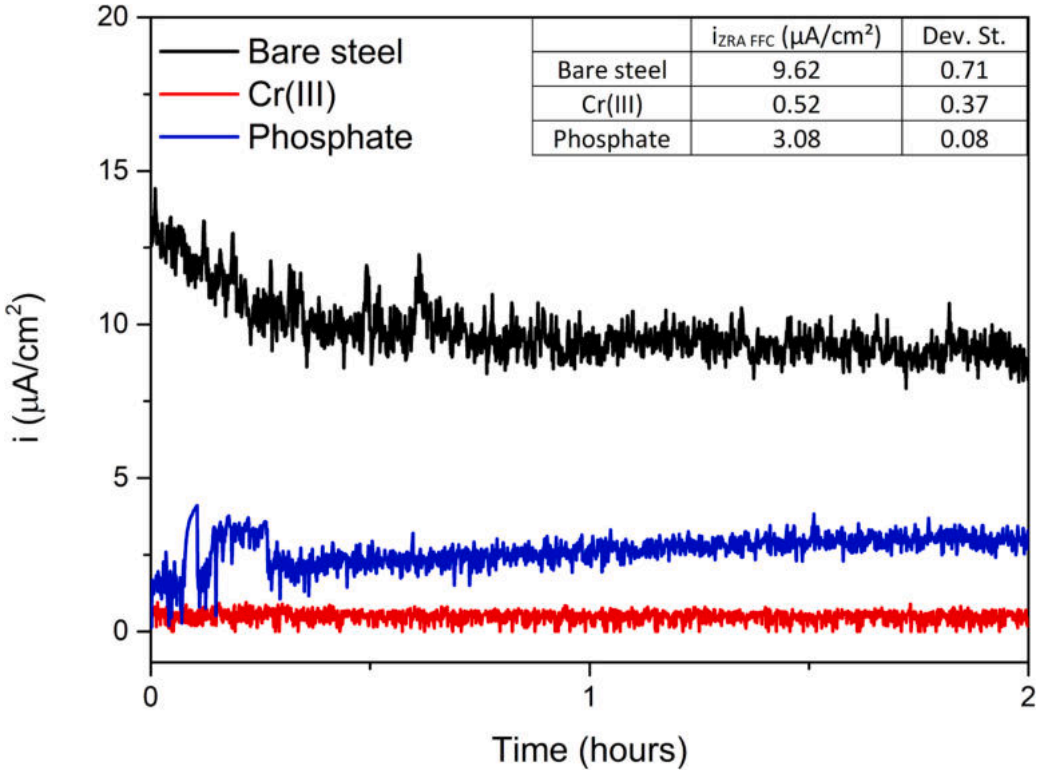

	$i_{ZRA\ FFC}$ (µA/cm²)	Dev. St.
Bare steel	9.62	0.71
Cr(III)	0.52	0.37
Phosphate	3.08	0.08

Fig. 7. ZRA measurement over 2 h of monitoring. The inset reports the mean values of ZRA current calculated over the results of the replicants.

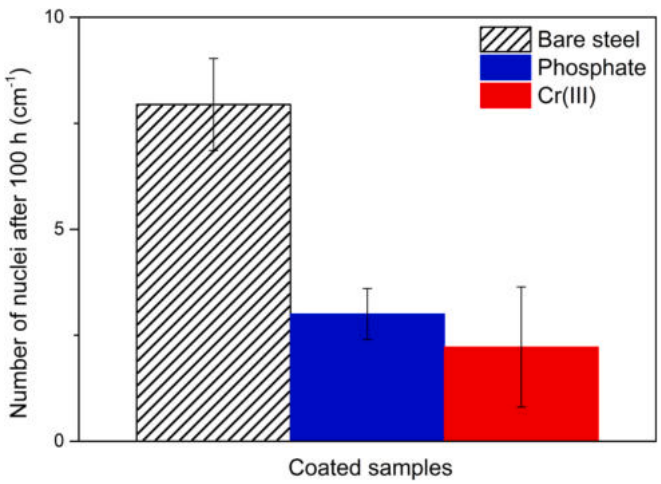

Fig. 9. FFC nucleation susceptibility evaluated at 100 h of filiform humidostatic test. Mean values over the three replicates testes samples per unit length.

between the three tested types of samples is provided in Fig. 10. The CCs seem able to display an enhanced wet adhesion, reducing the initiation sites for delamination. Previous studies report about the halo distributed around the scribe due to the cathodic activity formed when the samples are exposed to the neutral salt spray chamber during the initial contamination stage [8,9,60]. However, after its appearance and evolution during the contamination stage, there is a halt in further evolution because the distribution of contaminant ions triggers anodic undermining activity [8,61]. The initial presence of cathodic activity around the defect and its subsequent cessation is associated with the coupled anodic site. In this phase, cations produced from the solubilization of contaminant salts migrate toward the edges of the active region to counterbalance the negative charge generated by hydroxyl anions released during oxygen reduction at the cathodic front. This migration beneath the paint leads to the formation of an alkaline liquid film. As the deficiency of cations increases, iron cations (Fe^{2+} and Fe^{3+}) produced through steel dissolution fill the gap. The low solubility of iron hydroxides [62] hinders the movement of iron cations within the surrounding electrolyte. Upon depletion of cations from contaminants (such as Na^{+}, K^{+}) at the initially detached interface, the expansion of the cathodic region ceases, and a shift in the role of the reaction is observed toward an anodic undermining process [8,60]. As indicated by the arrows in Fig. 10, the presence of the conversion coatings mitigates the extent of this initial degradative activity. Based on these results, it is reasonable to assume that both Cr(III) and Phosphate exhibit strong performance in resisting cathodic delamination, in agreement with the simulated electrochemical results. The enhanced performances provided by CCs could rely on the greater paint adhesion which makes more difficult to damage the stronger metal-paint interface or form iron based compounds able to disadvantage the movement of charged species in the interfacial environment [14,56]. Keeping in mind the dual nature of the FFC mechanism and its initiation it is clear that a good mitigation strategy for FFC protection implies also a proper inhibitive action on cathodic delamination since it is strongly involved in the early stages of the phenomenon.

As suggested by the PDP's results, and in particular the superposition of the anodic branches in Fig. 6, the filament propagation is less influenced by the presence of the chemical conversion treatment. Since after FFC nucleation, the delamination front is anodic [2,10,60], the propagation cannot significatively be mitigated by CCs that are not stable in an acidic environment. The corroded area evolution with time is reported in Fig. 11a, in which the diagram representing the FFC growth rates is inserted. Even though Cr(III) displayed promising characteristics in the electrochemical tests regarding FFC driving forces acting on cathodic events (Fig. 6), it appears to be ineffective in mitigating the progression of FFC. On the other hand, Phosphate reduces the growth rate (by 32 %) and corroded area extension. After 270 h in a climatic chamber (Fig. 12), the samples treated by phosphating are less damaged. Currently, the predictive accuracy of propagation rates appears to be enhanced when relying on the R_{ct} values derived from electrochemical impedance spectroscopy (EIS) raw data modeling (Table 2). This

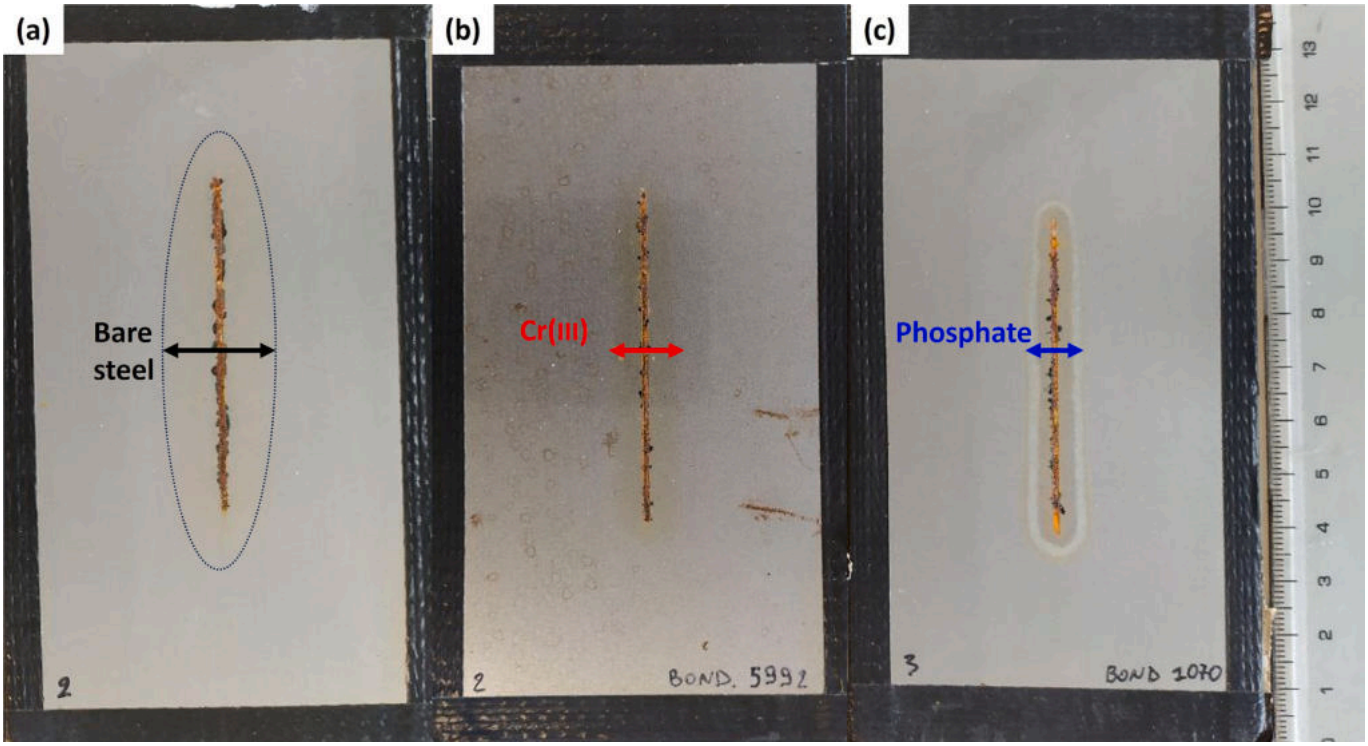

Fig. 10. Coated samples after 100 h of filiform test. The diverse extent of the cathodic halo developed during the first NSST contamination stage is highlighted.

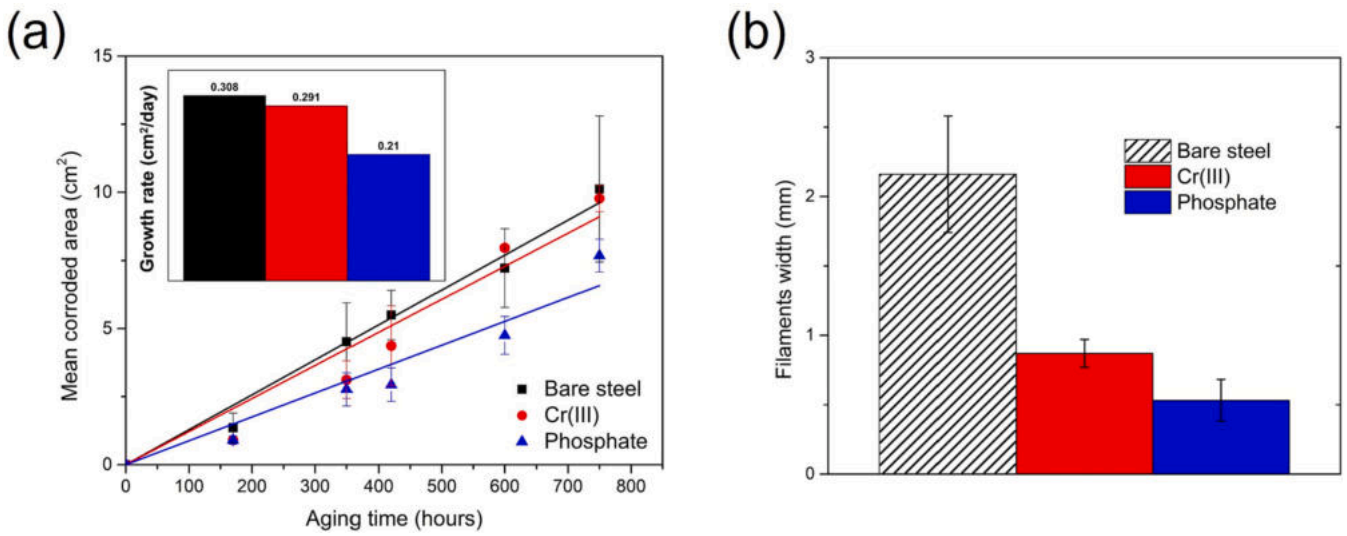

Fig. 11. Corroded area evolution over time (a) and average filaments width after 750 h of aging (b). The inset shows the propagation rates derived from the fitting lines.

parameter has proven effective in discerning subtle performance variations, potentially attributed to a less severe testing environment. Notably, the aggressive nature of the simulated acid anolyte conceals these characteristics. In instances involving the presence of a phosphate layer, a higher charge transfer resistance may underlie the restrained propagation of delamination. Concerning the durability of conversion coatings, their primary determinant lies in their capacity to withstand the harsh conditions arising at the interface between the metal and paint during the various steps of FFC evolution. Additionally, their pivotal role in impeding the movement of charged species is essential to decelerating the progression of the corrosive phenomenon. Also, the observed reduction in filament width in Fig. 11b for CCs compared to coated bare steel could be attributed to enhanced bonding.

Fig. 12 also shows the extent of damage at the conclusion of the 750 h filiform test. At this juncture, the chemical-physical compatibility between the organic coating and the treated surface significantly influences corrosion progression. This factor cannot be incorporated into an electrochemical simulated approach reliant on experiments conducted on uncoated substrates. The proposed methodologies are not independently applicable; instead, they require integration with wet adhesion tests in the specific scenario outlined. This necessity arises particularly when alterations occur in the metal-paint interface owing to surface modifications, such as conversion treatments. Nevertheless, the approach holds greater utility in comparing the FFC susceptibility of organic coated systems that share analogous interfacial interactions, such as similar alloys with diverse compositions [11], metals heat treatments [63], or paints containing varied inhibitors.

The steel conversion affects the FFC morphology. Fig. 13 shows the evolution of underpaint corrosion for the different samples. The filaments are well-developed and unidirectionally propagated for the Phosphate substrate (Fig. 13a); the painted Cr(III) conversion coating shows diffuse FFC ramifications in all directions (Fig. 13b). This change in morphology can be associated with the lower adhesion displayed by the Cr(III) layer and the acrylic-based layer. In situations where the paint bonding is weak, the growth of lateral branches appears to be promoted. In contrast, for the Phosphate coating, growth primarily occurs in the longitudinal direction, where there is a notable aeration gradient. When the adhesion is low the corrosion product formation yields the coating lift from the substrate [45], and if it is not enough bonded, some filaments could nucleate sideways. Concerning the organic coating in this context, its predominant influence stems from adhesion and interaction with the substrate. While oxygen and water permeability may pose potential concerns, their impact is not predominant when assessing the evolution of delamination initiated from a macrodefect. This is because the primary source of the species necessary for the reaction's progression is derived from the open defect and filament tails [6].

4. Conclusions

In this study, commercially available conversion coatings were tested for their ability to mitigate filiform corrosion (FFC) in acrylic-coated steel. Widely used technologies were selected, including trivalent chromium conversion and phosphating, and some novel insights specific to FFC mitigation in organic coated steel are presented. Their electrochemical response was assessed at first in a near-neutral environment. To simulate the FFC mechanism the converted surfaces were tested by means of simulated electrochemical approach coupling PDP and ZRA outcomes. The outcomes carried out with testing solutions reproducing the anolyte and catholyte environments developed in the FFC interface show that both conversion coatings are acting mainly inhibiting the cathodic events and seem less efficient in providing enhanced performances in the anodic acidic one.

The electrochemical findings did not fully match the actual corrosion resistance assessed on acrylic-coated samples in terms of FFC propagation. The main reasons responsible for the mismatch could be: (i) the main effects given by CCs were found on the cathodic event which is not the leading one once the filaments are formed, (ii) the cathodic reaction takes place on reactive sites that have already been damaged by the passage of the anodic front; this occurrence compromises the protection provided by the CCs, rendering it affected, (iii) the interfacial compatibility between the converted surfaces and the organic layer cannot be included in the electrochemical simulated method. However, a beneficial effect of the conversion treatments was highlighted during the cathodic-driven initiation phase for both the CCs, according to the electrochemical outcomes in an alkaline environment (PDP and ZRA).

In addition to corrosion performance, this study discussed the applicability of the experimental approach proposed in our previous publication [9], which is based on potentiodynamic polarization curves and zero-resistance ammeter to investigate conversion coatings. In the end, this approach should be considered as a supplementary method to the electrochemical characterization under near-neutral conditions when assessing the efficacy of conversion coatings. Since the protective performance of conversion coatings against FFC might not be as effective as for cathodic delamination, this novel approach has the potential to yield divergent results and therefore adds valuable insights to the evaluation process.

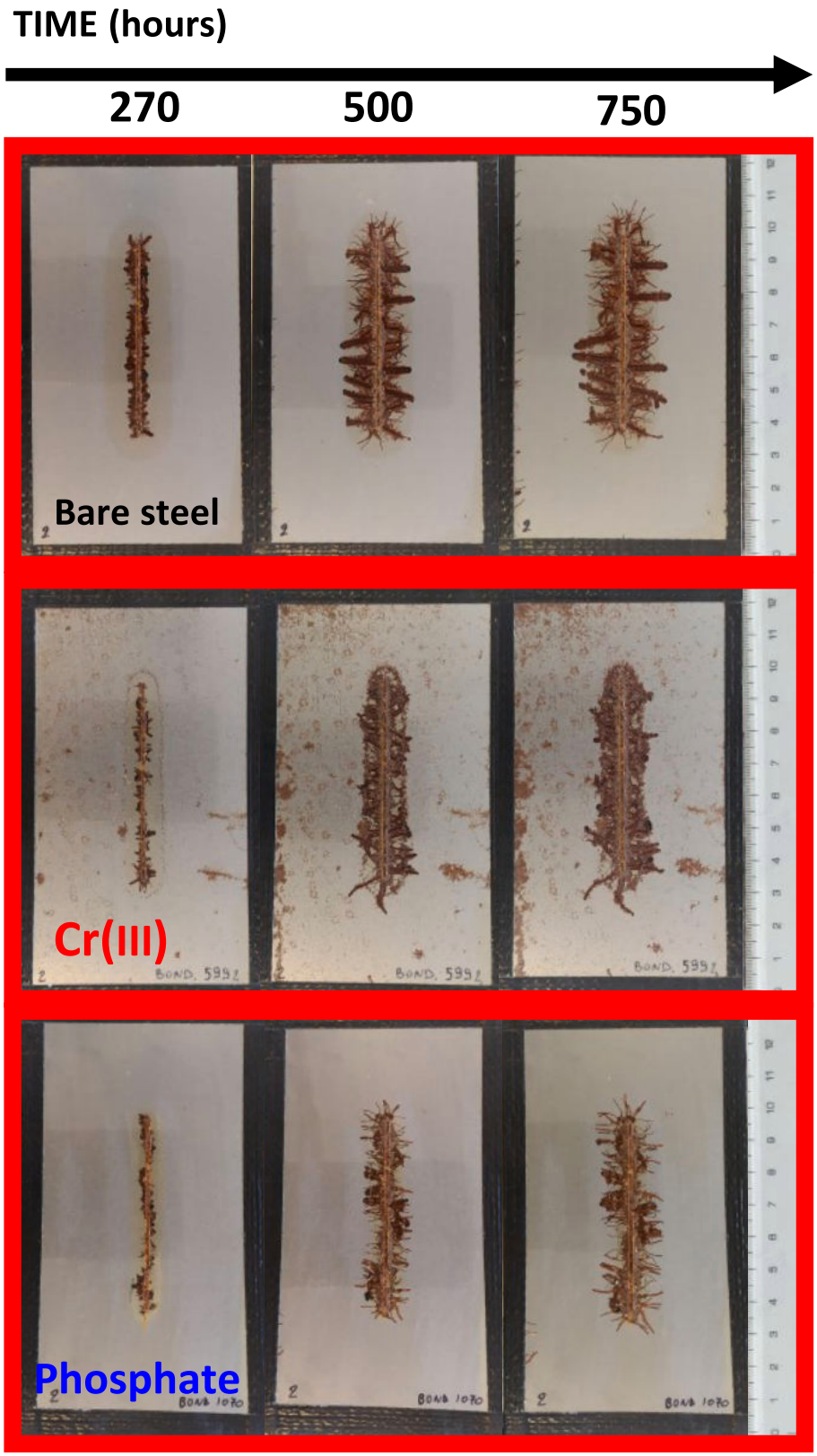

Fig. 12. Coated samples degradation after 270, 500, and 750 h of filiform humidostatic test.

CRediT authorship contribution statement

Andrea Cristoforetti: Writing – original draft, Methodology, Investigation, Formal analysis, Data curation, Conceptualization. **Stefano Rossi:** Writing – review & editing, Supervision, Resources, Project administration, Methodology. **Flavio Deflorian:** Supervision, Resources, Project administration. **Michele Fedel:** Writing – review & editing, Validation, Supervision, Resources, Project administration, Methodology.

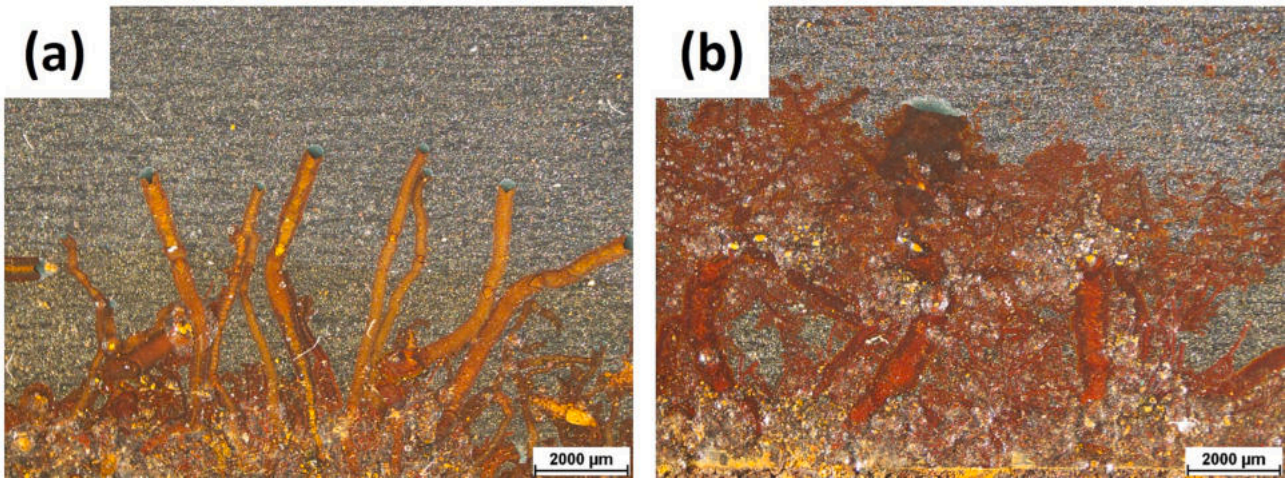

Fig. 13. Details of the modified FFC morphology caused by the conversion layers, phosphate (a) and Cr(III) (b). Images taken after 500 h of the filiform test.

Declaration of competing interest

The authors declare that they have no known competing financial interests or personal relationships that could have appeared to influence the work reported in this paper.

Data availability

Data will be made available on request.

Acknowledgment

The authors gratefully acknowledge Palini Vernici S.r.l and Henkel Italia S.r.l in particular Ludovico Palladini and Andrea Soldati.

Appendix A

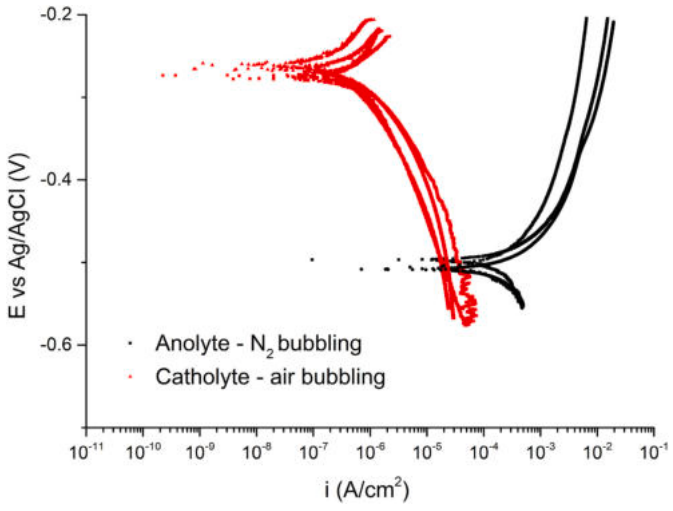

A1. Reproducibility of the polarization curves in anolyte and catholyte for bare steel substrate

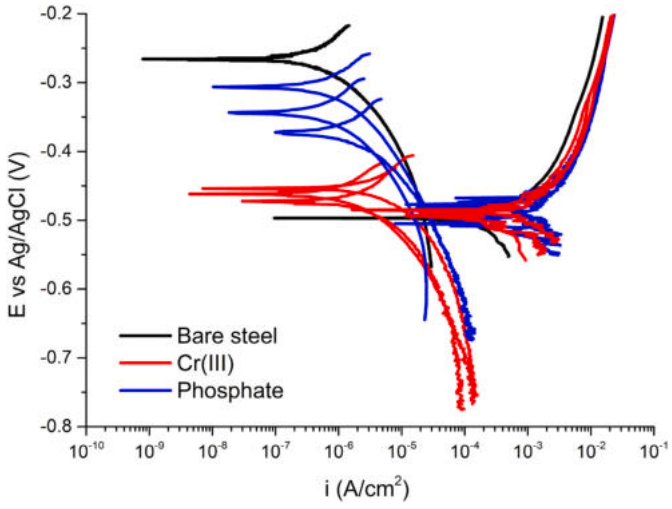

A2. Reproducibility of the polarization curves collected in anolyte and catholyte on treated steel substrate in comparison with the bare metal (blank)

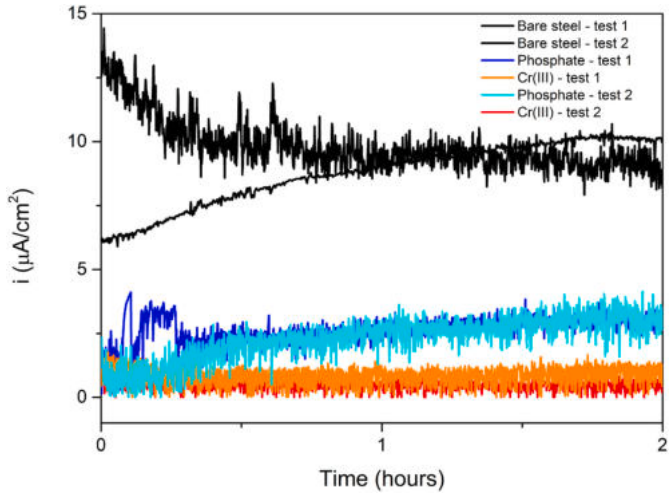

A3. Reproducibility of the ZRA curves collected in anolyte and catholyte on treated steel substrate in comparison with the bare metal

References

[1] C.F. Sharman, Filiform underfilm corrosion of lacquered steel surfaces, Nature 3890 (1944) 621–622.

[2] A. Bautista, Filiform corrosion in polymer-coated metals, Prog. Org. Coat. 28 (1996) 49–58, https://doi.org/10.1016/0300-9440(95)00555-2.

[3] S.H. Drissi, P. Refait, M. Abdelmoula, J.M.R. Génin, The preparation and thermodynamic properties of Fe(II) and Fe(III) hydroxide-carbonate (green rust 1), Pourbaix diagram of iron in carbonate-containing aqueous media, Corrosion Science 37 (1995) 2025–2041, https://doi.org/10.1016/0010-938X(95)00096-3.

[4] J.M.R. Génin, P.H. Refait, M. Abdelmoula, Green rusts and their relationship to iron corrosion; a key role in microbially influenced corrosion, Hyperfine Interact. 139–140 (2002) 119–131, https://doi.org/10.1023/A:1021219021919.

[5] R.T. Ruggeri, T.R. Beck, An analysis of mass transfer in filiform corrosion, Corrosion 39 (1983) 452–465, https://doi.org/10.5006/1.3581907.

[6] T.M. Watson, A.J. Coleman, G. Williams, H.N. McMurray, The effect of oxygen partial pressure on the filiform corrosion of organic coated iron, Corros. Sci. 89 (2014) 46–58, https://doi.org/10.1016/j.corsci.2014.08.004.

[7] M. Van Loo, D.D. Laiderman, R.R. Bruhn, Filiform corrosion, Corrosion 9 (1953) 277–283, https://doi.org/10.5006/0010-9312-9.8.277.

[8] A. Cristoforetti, F. Deflorian, S. Rossi, M. Fedel, On the occurrence of filiform corrosion on organic coated carbon steel exposed to cyclic aging test, Corrosion 79 (2023) 1339–1344, https://doi.org/10.5006/4443.

[9] A. Cristoforetti, S. Rossi, F. Deflorian, M. Fedel, An electrochemical study on the mechanism of filiform corrosion on acrylic-coated carbon steel, Prog. Org. Coat. 179 (2023) 107525, https://doi.org/10.1016/j.porgcoat.2023.107525.

[10] A. Cristoforetti, J. Izquierdo, R.M. Souto, F. Deflorian, M. Fedel, S. Rossi, In-situ measurement of electrochemical activity related to filiform corrosion in organic coated steel by scanning vibrating electrode technique and scanning micropotentiometry, Corros. Sci. 227 (2024) 111669, https://doi.org/10.1016/j.corsci.2023.111669.

[11] J.M.C. Mol, B.R.W. Hinton, D.H. Van Der Weijde, J.H.W. De Wit, S. Van Der Zwaag, A filiform corrosion and potentiodynamic polarisation study of some aluminium alloys, J. Mater. Sci. 35 (2000) 1629–1639, https://doi.org/10.1023/A:1004795528090.

[12] D.H. van der Weijde, E.P.M. van Westing, J.H.W. de Wit, EIS measurements on artificial blisters in organic coatings, Electrochim. Acta 41 (1996) 1103–1107, https://doi.org/10.1016/0013-4686(95)00444-0.

[13] Z. Gao, D. Zhang, X. Li, S. Jiang, Q. Zhang, Current status, opportunities and challenges in chemical conversion coatings for zinc, Colloids Surf. A Physicochem. Eng. Asp. 546 (2018) 221–236, https://doi.org/10.1016/j.colsurfa.2018.03.018.

[14] M.H. Shahini, H. Eivaz Mohammadloo, B. Ramezanzadeh, Recent advances in steel surface treatment via novel/green conversion coatings for anti-corrosion applications: a review study, J. Coat. Technol. Res. 19 (2022) 159–199, https://doi.org/10.1007/s11998-021-00466-0.

[15] Z. Gao, D. Zhang, Z. Liu, X. Li, S. Jiang, Q. Zhang, Formation mechanisms of environmentally acceptable chemical conversion coatings for zinc: a review, J. Coat. Technol. Res. 16 (2019) 1–13.

[16] V. Saarimaa, E. Kauppinen, A. Markkula, J. Juhanoja, B.-J. Skrifvars, P. Steen, Microscale distribution of Ti-based conversion layer on hot dip galvanized steel, Surf. Coat. Technol. 206 (2012) 4173–4179, https://doi.org/10.1016/j.surfcoat.2012.04.017.

[17] S. Hesamedini, A. Bund, Trivalent chromium conversion coatings, J. Coat. Technol. Res. 16 (2019) 623–641.

[18] D. Liu, Z. Yang, Z. Wang, C. Zhang, Synthesis and evaluation of corrosion resistance of molybdate-based conversion coatings on electroplated zinc, Surf. Coat. Technol. 205 (2010) 2328–2334, https://doi.org/10.1016/j.surfcoat.2010.09.018.

[19] C. Wang, F. Jiang, F. Wang, The characterization and corrosion resistance of cerium chemical conversion coatings for 304 stainless steel, Corros. Sci. 46 (2004) 75–89.
[20] A.R. Di Sarli, J.D. Culcasi, C. Tomachuk, C.I. Elsner, J. Ferreira-Jr, I. Costa, A conversion layer based on trivalent chromium and cobalt for the corrosion protection of electrogalvanized steel, Surf. Coat. Technol. 258 (2014) 426–436.
[21] I. Milošev, G.S. Frankel, Review—conversion coatings based on zirconium and/or titanium, J. Electrochem. Soc. 165 (2018) C127–C144, https://doi.org/10.1149/2.0371803jes.
[22] C.F. Glover, M.L.C. Lim, J.R. Scully, Increased filiform corrosion resistance utilizing a zirconium-based conversion coating on an Al-Zn-Mg-Cu (AA7075-T6) alloy as well as selected surface treatments, Corrosion 77 (2020) 40–52, https://doi.org/10.5006/3510.
[23] S. Zhang, B. Yang, G. Kong, J. Lu, Electrochemical analysis of molybdate conversion coating on hot-dip galvanized steel in various growth stages, Surf. Interface Anal. 49 (2017) 698–704.
[24] A. Cristoforetti, M. Fedel, F. Deflorian, S. Rossi, Influence of deposition parameters on the behavior of nitro-cobalt-based and Ti-hexafluoride-based pretreatments, J. Coat. Technol. Res. 19 (2021) 859–873, https://doi.org/10.1007/s11998-021-00563-0.
[25] A. Miszczyk, K. Darowicki, Water uptake in protective organic coatings and its reflection in measured coating impedance, Prog. Org. Coat. 124 (2018) 296–302, https://doi.org/10.1016/J.PORGCOAT.2018.03.002.
[26] A.S. Castela, A.M. Simões, Assessment of water uptake in coil coatings by capacitance measurements, Prog. Org. Coat. 46 (2003) 55–61, https://doi.org/10.1016/S0300-9440(02)00190-X.
[27] S. Akbarzadeh, M. Ramezanzadeh, B. Ramezanzadeh, Inspection the corrosion prevention performance and dry/wet interfacial adhesion qualities of the melamine-cured polyester coating applied on the treated mild steel surface with a nanostructured composite cerium-neodymium film, Colloids Surf. A Physicochem. Eng. Asp. 590 (2020) 124472.
[28] Z. Mahidashti, T. Shahrabi, B. Ramezanzadeh, The role of post-treatment of an ecofriendly cerium nanostructure conversion coating by green corrosion inhibitor on the adhesion and corrosion protection properties of the epoxy coating, Prog. Org. Coat. 114 (2018) 19–32.
[29] J.V. Kloet, W. Schmidt, A.W. Hassel, M. Stratmann, The role of chromate in filiform corrosion inhibition, Electrochim. Acta 48 (2003) 1211–1222, https://doi.org/10.1016/S0013-4686(02)00829-0.
[30] M. Fedel, C. Zanella, L. Ferrari, F. Deflorian, Effect of the synthesis parameters of in situ grown Mg-Al LDHs on the filiform corrosion susceptibility of painted AA5005, Electrochim. Acta 381 (2021) 138288, https://doi.org/10.1016/J.ELECTACTA.2021.138288.
[31] N. LeBozec, D. Persson, D. Thierry, S.B. Axelsen, Effect of climatic parameters on filiform corrosion of coated aluminum alloys, Corrosion 60 (2004) 584–593, https://doi.org/10.5006/1.3287763.
[32] A. Afseth, J.H. Nordlien, G.M. Scamans, K. Nisancioglu, Effect of heat treatment on filiform corrosion of aluminium alloy AA3005, Corros. Sci. 43 (2001) 2093–2109, https://doi.org/10.1016/S0010-938X(01)00014-2.
[33] A. Afseth, J.H. Nordlien, G.M. Scamans, K. Nisancioglu, Influence of heat treatment and surface conditioning on filiform corrosion of aluminium alloys AA3005 and AA5754, Corros. Sci. 43 (2001) 2359–2377, https://doi.org/10.1016/S0010-938X(01)00019-1.
[34] J.M.C. Mol, A.E. Hughes, B.R.W. Hinton, S. van der Zwaag, A morphological study of filiform corrosive attack on chromated and alkaline-cleaned AA2024-T351 aluminium alloy, Corros. Sci. 46 (2004) 1201–1224, https://doi.org/10.1016/j.corsci.2003.09.012.
[35] X. Zhou, G. Thompson, G. Scamans, The influence of surface treatment on filiform corrosion resistance of painted aluminium alloy sheet, Corros. Sci. 45 (2003) 1767–1777.
[36] A. Nazarov, A.-P. Romano, M. Fedel, F. Deflorian, D. Thierry, M.-G. Olivier, Filiform corrosion of electrocoated aluminium alloy: role of surface pretreatment, Corros. Sci. 65 (2012) 187–198.
[37] A.C. Bastos, M.G. Ferreira, A.M. Simões, Corrosion inhibition by chromate and phosphate extracts for iron substrates studied by EIS and SVET, Corros. Sci. 48 (2006) 1500–1512, https://doi.org/10.1016/j.corsci.2005.05.021.
[38] P. Zarras, J.D. Stenger-Smith, Chapter 3 - smart inorganic and organic pretreatment coatings for the inhibition of corrosion on metals/alloys, in: A. Tiwari, J. Rawlins, L.H. Hihara (Eds.), Intelligent Coatings for Corrosion Control, Butterworth-Heinemann, Boston, 2015, pp. 59–91, https://doi.org/10.1016/B978-0-12-411467-8.00003-9.
[39] ASTM, D2803-09, Standard Guide for Testing Filiform Corrosion Resistance of Organic Coatings on Metal, 2020, https://doi.org/10.1520/D2803-09R20.
[40] B. Ramezanzadeh, M. Attar, Effects of Co (II) and Ni (II) on the surface morphology and anticorrosion performance of the steel samples pretreated by Cr (III) conversion coating, Corrosion, The Journal of Science and Engineering 68 (2012) 015008-1.
[41] G. Williams, H.N. McMurray, D. Hayman, P.C. Morgan, Time-lapse potentiometric imaging of active filiform corrosion using a scanning Kelvin probe technique, PhysChemComm 4 (2001) 1–6, https://doi.org/10.1039/b100835h.
[42] G. Hoch, A Review of Filiform Corrosion, Localized Corrosion, NACE-3, Eds. RW Staehle, BF Brown, J. Kruger, A. Agrawal (Houston, TX) (1974).
[43] E.L. Koehler, Influence of contaminants on the failure of protective organic coatings on steel, Corrosion 33 (1977) 209–217, https://doi.org/10.5006/0010-9312-33.6.209.
[44] J.H.W. de Wit, New knowledge on localized corrosion obtained from local measuring techniques, Electrochim. Acta 46 (2001) 3641–3650, https://doi.org/10.1016/S0013-4686(01)00642-9.
[45] W.H. Slabaugh, M. Grotheer, Mechanism of filiform corrosion, Ind. Eng. Chem. 46 (1954) 1014–1016, https://doi.org/10.1021/ie50533a053.
[46] M. Pourbaix, J. Burbank, Atlas D-equilibres electrochimiques, J. Electrochem. Soc. 111 (1964) 14C.
[47] A. Cristoforetti, S. Rossi, F. Deflorian, M. Fedel, Comparative study between natural and artificial weathering of acrylic-coated steel, aluminum, and galvanized steel, Mater. Corros. 74 (2023) 1429–1438, https://doi.org/10.1002/maco.202313858.
[48] ASTM B117-19, Standard Practice for Operating Salt Spray (Fog) Apparatus, 2019, https://doi.org/10.1520/B0117-19.
[49] S. Jain, M. Lim, J. Hudson, J. Scully, Spreading of intergranular corrosion on the surface of sensitized Al-4.4 Mg alloys: a general finding, Corros. Sci. 59 (2012) 136–147.
[50] N. Debnath, Importance of surface preparation for corrosion protection of automobiles, Journal of Surface Engineered Materials and Advanced Technology 03 (2013) 94–105, https://doi.org/10.4236/jsemat.2013.31A014.
[51] J.P. Popić, B. Jegdić, J. Bajat, D. Veljovic, S. Stevanovic, V. Miskovic-Stankovic, The effect of deposition temperature on the surface coverage and morphology of iron-phosphate coatings on low carbon steel, Appl. Surf. Sci. 257 (2011) 10855–10862, https://doi.org/10.1016/j.apsusc.2011.07.122.
[52] A. Ghanbari, M.M. Attar, The effect of zirconium-based surface treatment on the cathodic disbonding resistance of epoxy coated mild steel, Appl. Surf. Sci. 316 (2014) 429–434, https://doi.org/10.1016/j.apsusc.2014.07.178.
[53] L. Razzaboni, L. Casanova, M. Pedeferri, M. Ormellese, A green vanadium-based formulation for the conversion of steel, Surf. Eng. 39 (2023) 613–624.
[54] J.-B. Jorcin, M.E. Orazem, N. Pébère, B. Tribollet, CPE analysis by local electrochemical impedance spectroscopy, Electrochim. Acta 51 (2006) 1473–1479, https://doi.org/10.1016/j.electacta.2005.02.128.
[55] B. Hirschorn, M.E. Orazem, B. Tribollet, V. Vivier, I. Frateur, M. Musiani, Determination of effective capacitance and film thickness from constant-phase-element parameters, Electrochim. Acta 55 (2010) 6218–6227.
[56] G. Klimow, N. Fink, G. Grundmeier, Electrochemical studies of the inhibition of the cathodic delamination of organically coated galvanised steel by thin conversion films, Electrochim. Acta 53 (2007) 1290–1299, https://doi.org/10.1016/j.electacta.2007.05.045.
[57] E.R. Vago, K. de Weldige, M. Rohwerder, M. Stratmann, Electroreduction of oxygen on octadecylmercaptan self-assembled monolayers, Fresenius J. Anal. Chem. 353 (1995) 316–319, https://doi.org/10.1007/BF00322059.
[58] F. Deflorian, L. Fedrizzi, Adhesion characterization of protective organic coatings by electrochemical impedance spectroscopy, J. Adhes. Sci. Technol. 13 (1999) 629–645, https://doi.org/10.1163/156856199X00154.
[59] D.Y. Perera, On adhesion and stress in organic coatings, Prog. Org. Coat. 28 (1996) 21–23, https://doi.org/10.1016/0300-9440(95)00585-4.
[60] G. Williams, H.N. McMurray, The mechanism of group (I) chloride initiated filiform corrosion on iron, Electrochem. Commun. 5 (2003) 871–877, https://doi.org/10.1016/J.ELECOM.2003.08.008.
[61] G. Williams, R. Grace, Chloride-induced filiform corrosion of organic-coated magnesium, Electrochim. Acta 56 (2011) 1894–1903, https://doi.org/10.1016/J.ELECTACTA.2010.09.005.
[62] J.D.B. Sharman, J.M. Sykes, T. Handyside, Cathodic disbonding of chlorinated rubber coatings from steel, Corros. Sci. 35 (1993) 1375–1383.
[63] J.M.C. Mol, J. van de Langkruis, J.H.W. de Wit, S. van der Zwaag, An integrated study on the effect of pre- and post-extrusion heat treatments and surface treatment on the filiform corrosion properties of an aluminium extrusion alloy, Corros. Sci. 47 (2005) 2711–2730, https://doi.org/10.1016/j.corsci.2004.11.003.
[65] M. Fedel, S. Zonta, A. Cristoforetti, Study of ZnAl Hydroxides-Based Thin Films to Enhance the Filiform Corrosion Resistance of Acrylic-Coated AA5005, J. Electrochem. Soc. 171 (2024) 021501, https://doi.org/10.1149/1945-7111/ad2599.